IEEE Access
Multidisciplinary | Rapid Review | Open Access Journal

Received December 5, 2018, accepted December 26, 2018, date of publication January 10, 2019, date of current version February 6, 2019.

Digital Object Identifier 10.1109/ACCESS.2019.2891958

Incision Sensor Using Conductive Tape for Cricothyrotomy Training Simulation With Quantitative Feedback

BUMMO AHN[1,2], WOONJAE CHOI[1,2], MARK P. OTTENSMEYER[3,4], AND HOERYONG JUNG[5]

[1]Robotics Research and Development Group, Korea Institute of Industrial Technology, Ansan-si 15588, South Korea
[2]Department of Robotics and Virtual Engineering, University of Science and Technology, Ansan-si 34113, South Korea
[3]Medical Device and Simulation Laboratory, Department of Radiology, Massachusetts General Hospital, Cambridge, MA 02139, USA
[4]Harvard Medical School, Boston, MA 02115, USA
[5]Department of Mechanical Engineering, Konkuk University, Seoul 05029, South Korea

Corresponding author: Hoeryong Jung (junghl80@konkuk.ac.kr)

ABSTRACT Cricothyrotomy procedures, involving risky incisions on the neck skin and internal membranes, require rigorous training. In this paper, a novel incision sensor measuring the incision path in a cricothyrotomy training simulation is proposed. The sensor provides quantitative feedback to trainees on their incision practice, enhancing the effectiveness of the simulation. The sensor measures the electric potential, which decreases monotonically along the direction of current flow on the conductive material at the incision point, and converts it to coordinate values, based on the relationship between the electric potential and the position. The sensor comprises three layers of conductive tape, which are electrically isolated by two dielectric layers, and is fabricated as a thin film. The first two conductive layers (driving layers) are alternately energized to create distributions of electric potential in the x or y directions across the sensor plane. The third conductive layer (sensing layer), placed under the driving layers, transfers the electric potential to the output channel of the sensor at the point where a metal blade creates a short circuit between the energized driving layer and the sensing layer. The alternating measurements are converted to x and y coordinates of the incision position. The experiments for characterization and performance validation were performed using sensor prototypes fabricated with the proposed design and fabrication procedures. The experimental results show that the proposed sensor facilitates the measurement of the incision paths aligned with and diagonal to the x and y axes within root mean square errors of 0.98 and 1.03 mm, respectively.

INDEX TERMS Conductive tape, cricothyrotomy simulation, incision sensor, medical simulation.

I. INTRODUCTION

Surgical cricothyrotomy is an emergency procedure that is performed to establish an external airway for the patient in cases of life-threatening airway obstruction. In this procedure, doctors make consecutive incisions through the skin that covers the larynx and the cricothyroid membrane. Then they insert an endotracheal or tracheostomy tube through the opening to secure the airway [1]. It is generally performed when oral or nasal intubation cannot be performed (e.g., due to facial trauma) and is simpler and faster to perform than a tracheotomy [2]. The procedure is straightforward and can be completed in a few minutes, but it requires careful attention and rigorous airway management skills because it is a life-saving procedure performed as a last resort on a patient facing imminent death. When the procedure fails, the result is usually poor survival or neurologic devastation.

One of the main causes of failure is lack of clinical experience [3]. Because cricothyrotomy is an infrequently performed emergency procedure, regular refresher training is necessary for skill retention and maintenance [4], [5]. Cricothyrotomy training is conducted on models that mimic the human anatomy, which include mannequins [6], cadavers [7], [8], homemade models [9], animal models [10], [11], and simulators [12]–[17]. In these training modalities, trainees repeatedly practice the cricothyrotomy procedure on the replica, generally with instructor feedback, and improve their skills progressively as they begin to understand their errors and the corresponding consequences. Considering this learning mechanism, providing appropriate feedback to trainees is important to guide them correctly through the practical skills and enhance training effectiveness. Similarly, recognizing and pointing out errors further accelerates

the learning curve. Most cricothyrotomy trainers, however, do not provide integrated feedback due to the absence of suitable sensors that would evaluate the trainee's skills.

The most critical step in cricothyrotomy is the incision procedure on the neck skin and cricothyroid membrane. It should be performed precisely, carefully avoiding unnecessary damage to the nearby cricothyroid muscles, recurrent laryngeal nerves, carotid arteries, and internal jugular veins. In addition, the allowable margin for error is narrow, and mistakes can lead to serious consequences. The patient may suffer from complications such as speech disorders, or their life could be at risk due to a misplaced incision. Thus, physicians should undergo rigorous training to acquire precise incision skills. Most of the cricothyrotomy simulators provide an interface to practice this incision procedure, but the simulators do not provide appropriate feedback on the incision performance. The absence of feedback degrades the training effectiveness of cricothyrotomy simulators. There have been numerous studies for developing sensors to measure position information on artificial skin [18]–[24], but no sensors have been developed for incision measurement.

In this study, we propose a novel incision sensor to measure the coordinates of incisions (incision path) made on the synthetic skin of a mannequin in a cricothyrotomy simulator. The proposed incision sensor facilitates objective and quantitative feedback regarding the extent of longitudinal and directional errors compared to the reference path of the incision. Trainees can be informed about the results of their incision practice attempts precisely using the proposed incision sensor; thus, it enhances the training effectiveness of the cricothyrotomy simulator. The incision sensor is fabricated in a thin-film form with three layers of conductive tape, which are electrically isolated from each other by dielectric layers. The sensor is placed under the synthetic skin of the mannequin and incised, together with the skin, using an electrically conductive blade, to measure the two-dimensional (2D) coordinates of the incision path. The sensor measures the electric potential on the conductive tape at the incision point and converts it to coordinate values with respect to the sensor-attached coordinate frame, using a predefined relationship between the electric potential and the coordinate values. The experiments for characterization and performance validation of the sensor were conducted with sensor prototypes fabricated with the proposed design and fabrication procedure. The experimental results demonstrate the feasibility of the sensor and its applicability to cricothyrotomy simulation in measuring the incision path made by the trainee.

II. DESIGN AND FABRICATION

A. SYSTEM OVERVIEW OF CRICOTHYROTOMY TRAINING SIMULATOR

Fig. 1(a) shows two incisions performed in the cricothyrotomy procedure. The physician makes a 3–5 cm vertical incision between the thyroid cartilage and cricoid cartilage and a 1-cm horizontal incision on the cricothyroid membrane [25]. Fig. 1(b) shows a training simulator implementing the proposed sensor. Mannequins (ALS Simulator, head (item number 205-03250) with airway & tongue assembly (200-03150), Laerdal, Wappingers Falls, NY, USA) replicating the laryngeal anatomy of humans are employed, and two incision sensors are attached to the parts of the mannequin corresponding to the neck skin and the cricothyroid membrane. The incision sensor dimensions and locations cover the possible region of incision under the assumption that trainees have basic knowledge of the laryngeal anatomy and incision procedure [26]. The incision sensor is placed under the synthetic skin of the mannequin, concealing it from the trainee. Once the trainee makes an incision on the skin of the mannequin, the incision sensor under the skin is incised together with the skin and measures the path of the incision. The measured incision path is graphically presented to the trainee, with the ideal path as reference, providing a concrete illustration of how much error occurred in the incision, as shown in Fig. 1(c).

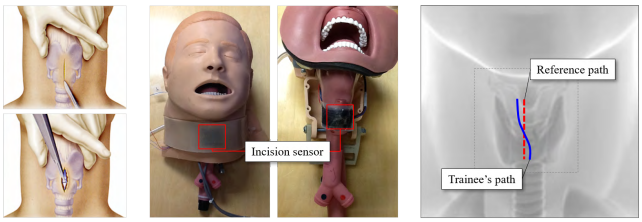

FIGURE 1. Overview of the cricothyrotomy training simulator. (a) Two incisions performed in the cricothyrotomy procedure. (b) The cricothyrotomy training simulator employing mannequins and two incision sensors. (c) Graphical feedback on the results of the incision practice.

B. INCISION SENSOR WITH CONDUCTIVE TAPE

To use the incision sensor in the cricothyrotomy training simulator, the following requirements should be satisfied. First, the sensor should be in the form of a thin film that can be placed under the synthetic skin of the mannequin and should be easily incised without causing additional resistive force. Second, high-fidelity sensors are preferred for generating training results, and thus, the sensor should be suitable for the accurate and precise measurement of the incision path. Third, it should be made of an inexpensive material because incising the sensor (and skin) is a destructive process, requiring the disposal of the sensor after use. Electrically conductive tape with a known resistivity was selected as the basic material for fabricating the incision sensor, because it is a thin and easily incised material. In addition, it is very inexpensive as a sensor material and can be used for incision path measurement with the following, simple principle.

The principle involves calculating the incision position by relating it to the value of the electric potential on the conductive tape at that point. If a voltage source is connected along one edge of a rectangular piece of conductive tape and the other edge is connected to ground, a gradient in

the electric potential is created along the tape with potential decreasing along the direction of current flow. The value of the electric potential can be mapped to the position on the conductive tape. Fig. 2 shows a rectangular conductive tape that is connected to a voltage source and ground through the electrodes attached at the left and right edges of the tape. When one pierces a point on the conductive tape using a sharp and conductive incision tool, the position of the piercing point can be estimated using the value of the electric potential.

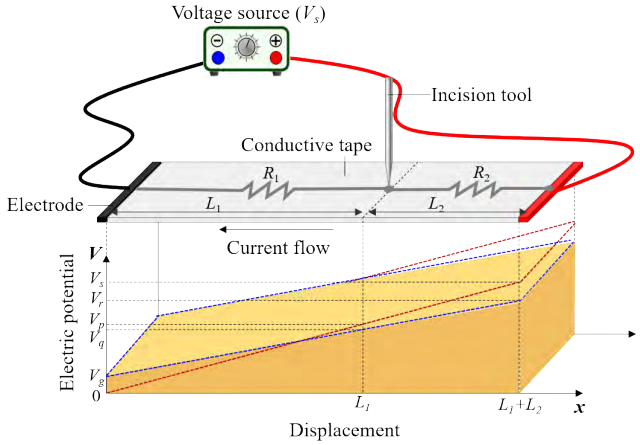

FIGURE 2. Principle of incision measurement using conductive tape. The red dotted line indicates the value of electric potential on the conductive tape in the ideal case, and the blue dotted line indicates the value of electric potential in the real case considering the voltage drop caused by other components in the circuit.

In Fig. 2, the conductive tape can be regarded as two resistors that are serially connected at the piercing point; essentially a voltage divider or potentiometer. R_1 and R_2 are the resistance values of the conductive tape segment on the left and right side of the piercing point, respectively. Assuming that the conductive tape is a homogeneous material and the electric potential drops only on the conductive tape in the circuit, the electric potential at the piercing point can be calculated as follows:

$$V_p = \frac{R_1}{R_1 + R_2} V_s \tag{1}$$

where V_p is the electric potential at the piercing point; V_s is the output voltage of the source; and R_i is the resistance value of the conductive tape segment, whose length is L_i. The resistance of the conductive tape segment is determined by Pouillet's law, $R = \rho L/A$ where ρ, L, and A are the electric resistivity, length, and cross-sectional area of the conductive tape, respectively. Then, the distance between the electrode connected to ground and the piercing point, which is denoted as L_1 in the figure, is calculated as follows:

$$L_1 = \frac{V_p}{V_s} L \tag{2}$$

where $L = L_1 + L_2$. This implies that the electric potential on the conductive tape varies linearly according to the distance between the electrode and the piercing point, and this can be used for the measurement of the one-dimensional (1D) position on the conductive tape. We assume that the electric potential drop occurs only on the conductive tape, as shown with the red dotted line in Fig. 2, but in a real implementation, a certain portion of the electric potential drops across other components of the circuit, such as electric wires, electrodes, and junctions between the electrodes and conductive tape. Accordingly, the value of the electric potential on the conductive tape would be the blue dotted line presented in Fig. 2. V_r and V_g denote the electric potential at the right and left ends of the conductive tape, respectively. The values of the electric potential at both ends of the conductive tape are recorded during calibration following sensor fabrication and are used to calculate the distance as follows:

$$L_1 = \frac{V_q}{V_r - V_g} L \tag{3}$$

where V_q is the electric potential at the piercing point in a real sensor. Then, the distance from the electrode to any point on the conductive tape can be estimated by using (3) with the electric potential measured at the point.

C. SENSOR AND CIRCUIT DESIGN

Fig. 3(a) shows the structure of the basic incision sensor module, which is used to measure the 1D incision path. The sensor module is composed of three layers: the driving layer, dielectric layer, and sensing layer. The driving layer is made of a conductive tape, and it is responsible for producing electric potentials across the incision sensor. Two electrodes, having low impedance connections to the ground and voltage sources, are attached at the left and the right edges of the rectangular conductive tape, respectively. The electric potential is the lowest at the left end of the driving layer and increases linearly along the direction opposite to the current flow, which is denoted by x in the figure. The value of the electric potential reaches its highest value at the right end of the layer. The dielectric layer, which is made of plastic tape, electrically isolates the driving layer from the sensing layer. There is no electric connection between the driving layer and sensing layer if there is no incision. The sensing layer is made of conductive tape and is responsible for transferring the electric potential on the driving layer at the incision point to a high-impedance analog input channel for analog to digital conversion. Fig. 3(b) shows the electric circuitry representing the incision sensor module undergoing incision. Once all layers of the sensor module are completely penetrated by the conductive incision tool, the driving layer is electrically connected to the sensing layer through the incision tool at the incision point, and the electric potential on the driving layer is transferred to the output channel of the sensor through the sensing layer. The conductive tapes and incision tool that are subject to current flow can be represented as resistances in the circuit diagram, as shown in Fig. 3(b). In the circuit diagram, R_s represents the resistance between the voltage source and the right end of the conductive tape, and R_g represents the resistance between ground and the left end of the conductive

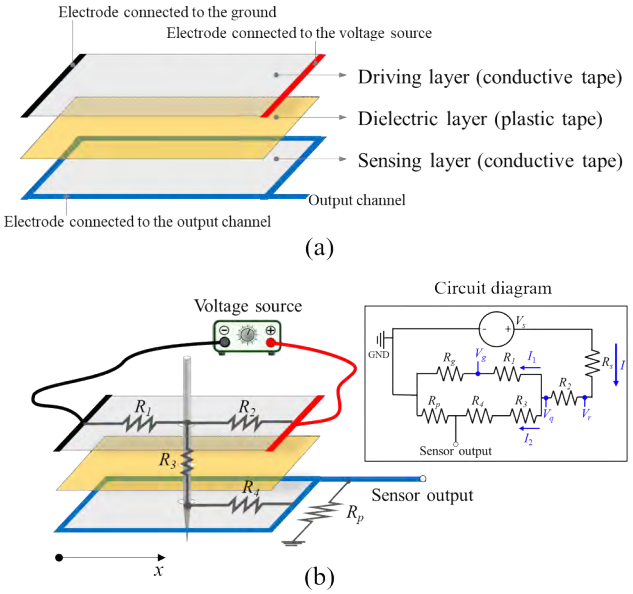

FIGURE 3. Design principle of the incision sensor. (a) Composition of the basic incision sensor module for measuring 1D incision coordinates. (b) Incision sensing mechanism transferring electric potential from the driving layer to the sensing layer in case of incision.

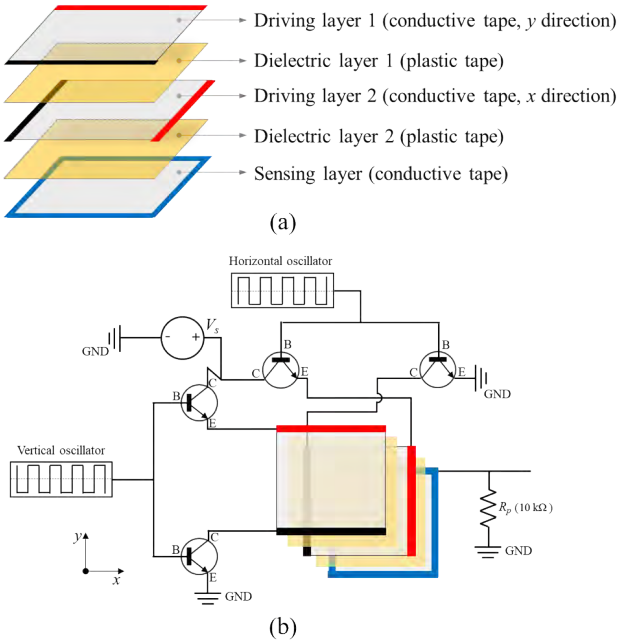

FIGURE 4. Design of the incision sensor. (a) Design of the incision sensor composed of three conductive layers and two dielectric layers. (b) Electric circuit diagram of the incision sensor.

tape. These resistances lead to additional voltage drops outside the sensor, resulting in reduced electric potential range ($V_r - V_g$) in the driving layer. The current through the circuit is represented as follows:

$$I = \frac{V_r - V_q}{R_2} \tag{4}$$

$$I_1 = \frac{V_q}{R_1 + R_g} \tag{5}$$

$$I_2 = \frac{V_q}{R_3 + R_4 + R_p} \tag{6}$$

where I is the total current through the circuit ($I = I_1 + I_2$); I_1 and I_2 are the current flows through the driving layer to the left side of the piercing point and through the sensor output, respectively; and V_q is the electric potential measured at the piercing point on the driving layer. To prevent the voltage measured at the output channel from floating randomly when there is no piercing tool, a pull-down resistor brings the sensing layer voltage to ground, which is distinct from the minimum voltage that would be measured during incision (V_g). The pull-down resistance is set to be much larger ($R_p = 10\,\text{k}\Omega$) than the resistance of the conductive tape ($< 50\Omega$), so that most of the current flows through the driving layer ($I_1 \gg I_2$). Only microcurrents flow through the tool and the sensing layer to transfer the electric potential to the output channel of the sensor, connected in turn to a high impedance analog to digital input channel. The electric potential at the incision point is measured in this manner, and distance x from the left end of the sensor to the incision point is calculated using (3).

Fig. 4 (a) shows the full structure of the incision sensor, which can measure a 2D incision path. The incision sensor is composed of three conductive layers (two driving layers and one sensing layer) and two dielectric layers. The sensing mechanism is the same as that of the 1D incision sensor module, with the additional feature that the edge conductors can be placed in either a driving or high-impedance state. Driving layers 1 and 2 produces an electric potential on the incision sensor in the y and x directions, respectively, in the sensor-attached coordinate frame, shown in Fig. 4(b). Once the sensor is completely penetrated by the incision tool, the electric potentials alternating between driving layers 1 and 2 are transmitted to the sensing layer through the incision tool. To measure the two electric potentials corresponding to the x and y directions using one sensing layer, an electric switching mechanism is employed, as shown in Fig. 4(b). Two electronic oscillators that create a square wave of 200 Hz are connected to driving layers 1 and 2. The oscillators periodically disconnect the current flow in the driving layers. The driving layer is connected to the voltage source and the ground only when it receives a high signal from the oscillator. By using the inverse form of the square waves, the two driving layers are alternatively activated. The electric potentials on driving layers 1 and 2 transferred to the sensing layer are sampled at 200 Hz, after some delay following the switch between layer activation, avoiding crosstalk between the x and y measurements. In this way, the sensor outputs the 2D coordinates of the incision point at 100 Hz, which is sufficient for capturing details of the incision path made in the cricothyrotomy simulation.

D. INCISION SENSOR FABRICATION

The incision sensor is fabricated using the suggested design presented in the previous section. The fabrication steps for the incision sensor are displayed in Fig. 5.

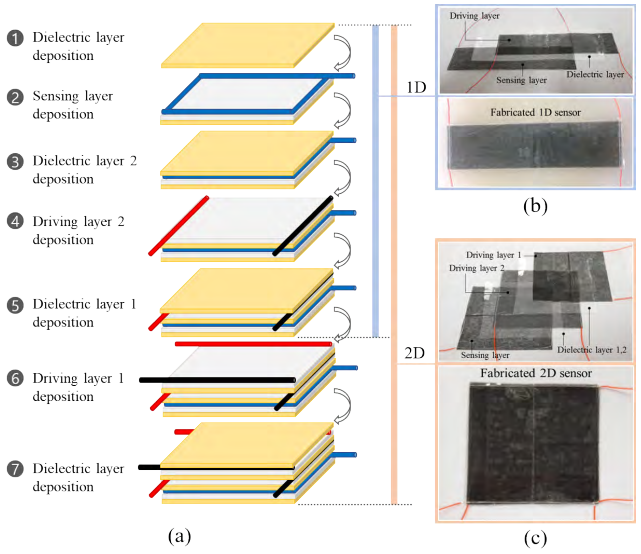

FIGURE 5. Incision sensor fabrication procedure. (a) Step-by-step fabrication procedure of the incision sensor. (b) Fabrication of prototypes of the 1D incision sensor module. (c) Fabrication of prototypes of complete incision sensor for 2D incision measurement.

Step 1: a plastic adhesive tape (370A ScotchTM Tape (Transparent), 3M Co., Maplewood, MN, USA) is placed on a flat jig, adhesive side up, as a base dielectric layer.

Step 2: a conductive adhesive tape (9712-1"X36YD, Electrically Conductive Adhesive Transfer Tape, 3M Co., Maplewood, MN, USA) is placed on the base layer. An electric wire (30 AWG, solid core, stripped of insulation where contact is made with the conductive tape) connected as an electrode to the output channel of the sensor is attached to all edges of the conductive tape. The wire is also fixed to the tape by the adhesive material on the tape. The conductive tape surrounded by the electric wire forms the sensing layer.

Step 3: dielectric layer 2, made of plastic adhesive tape, is laid on the sensing layer.

Step 4: another conductive adhesive tape layer is laid on dielectric layer 2, and two electric wires (stripped where is made with the conductive tape) are attached on the left and right edges of the conductive tape as electrodes connected to their respective control transistors. This layer forms driving layer 2.

Step 5: a plastic adhesive tape is deposited again to cover the sensor. At this point, the fabrication of the incision sensor module is complete.

Fig. 5(b) shows the fabricated prototype of the 1D incision sensor module. To extend the 1D incision sensor module for 2D incision measurement, additional conductive adhesive tape is laid on the module, and two electric wires are attached on the top and bottom edges of the conductive tape. This layer forms driving layer 1 (*Step 6*). Finally, plastic adhesive tape is laid on driving layer 1 (*Step 7*). Fig. 5(c) shows a fabricated prototype of the incision sensor that measures the 2D incision path.

E. SENSOR EQUIVALENT CIRCUIT

The incision sensor measures the incision position on the sensor coordinate frame using the value of electric potential on the two driving layers. Thus, the relation between the electric potential and the position on the sensor coordinate frame should be precisely modeled and verified to ensure the reliability of the sensor. Fig. 6(a) shows the schematic diagram of a driving layer, which is composed of a voltage source, two transistors, two electrodes, conductive tape, and an oscillator. The equivalent circuit model of the driving layer is shown in Fig. 6(b). In this circuit model, R_t represents the resistance of the conductive tape, R_c represents the contact resistance that occurs at the junction between the conductive tape and the electrode. The contact resistances are introduced to model the additional voltage drop at the junction between the electrode and the conductive tape. R_{tr1} and R_{tr2} are equivalent resistances introduced to model voltage drop through the transistors. Complicated electrical behavior involved in the transistor is simplified with the equivalent resistances since only the voltage drop is necessary to model the electric potential and the position on the conductive tape. Current i_t is the electric current flowing into the circuit. To convert the value of the electric potential at the incision point (V_q) into the position (L_1) using (3) requires knowledge of the value of the electric potentials at both sides of the conductive tape, denoted as V_r and V_g in the electric circuit model. V_r and V_g can be computed as follows:

$$V_r = V_s - V_{tr1} - V_{c1} \tag{7}$$

$$V_g = V_{c2} + V_{tr2} \tag{8}$$

where V_{c1} and V_{c2} are the voltage drops caused by the contact resistance at the junction of the electrode and conductive tape. Assuming that the contact resistances are the same at both junctions, V_{c1} and V_{c2} can be computed as follows:

$$V_{c1} = V_{c2} = i_e R_c. \tag{9}$$

Contact resistance R_c is experimentally measured using the method of transmission line measurements (TLM), and the experimental results are presented in following section. V_{tr1} and V_{tr2} are the voltage drops caused by the transistors connected to the voltage source and the ground respectively, and those values are experimentally measured ($V_{tr1} = 1.2\ V$, $V_{tr2} = 0.4\ V$).

F. CONTACT RESISTANCE MEASUREMENT

The contact resistance that arises at the junction between the conductive tape and the electrodes causes an additional voltage drop that affects the value of the electric potential at both ends of the conductive tape (V_r, V_g). The TLM method, which is widely used to determine the contact resistance between a metal and a semiconductor, is used to determine the

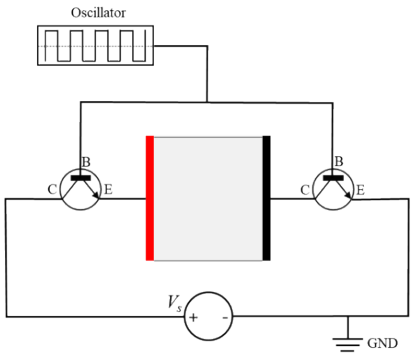

(a)

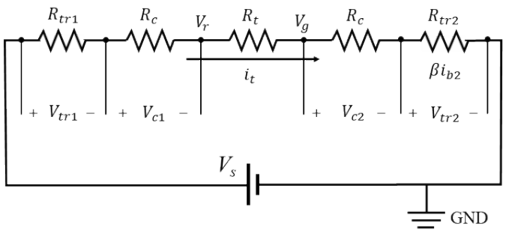

(b)

FIGURE 6. Schematic diagram and equivalent circuit model of the driving layer. (a) Schematic diagram of the driving layer. (b) Equivalent circuit model of the driving layer.

contact resistance experimentally [27], [28]. In this method, one measures the total resistance of a conductive material of various lengths, including contact junctions, and estimates the contact resistance with the measured resistance value. The total resistance of the conductive material can be expressed as follows:

$$R_T = 2R_c + \frac{R_{sh}}{W}L \tag{10}$$

where R_T is the measured total resistance, R_c is the contact resistance, R_{sh} is the sheet resistance of the conductive material, and W and L are the width and length of the conductive material, respectively. R_T was measured for 5 lengths (20, 40, 60, 80, 100 mm) and 3 widths (12.5, 25, 50 mm) of conductive tape, including two electrode junctions. Fig. 7 shows the experimental results. The sheet resistance R_{sh} was calculated by using the slope of the linear regression of the experimental data. The value of R_{sh} was 9.6Ω, 9.5Ω and 9.0Ω in the 12.5-mm, 25-mm and 50-mm wide conductive tape, respectively. Ideally, the R_{sh} should be same for those three conductive tapes, but there exist variations because of uncertain errors of the experiments. The value of contact resistances were experimentally determined as 7.10Ω, 3.65Ω and 2.85Ω for the 12.5-mm, 25-mm, and 50-mm wide conductive tapes, respectively. Theoretically, the contact resistance should be inversely proportional to the contact area, but the experimental results did not exactly match the theory because of

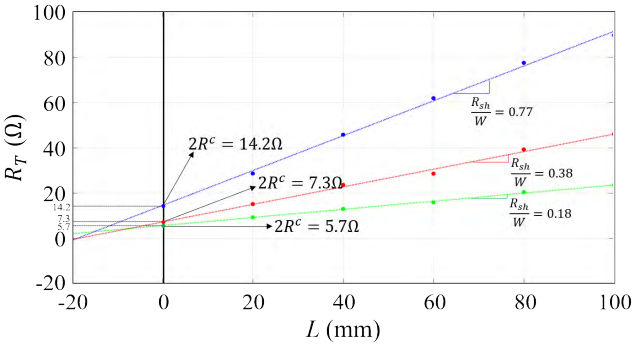

FIGURE 7. Experimental results of contact resistance measurement.

uncertain errors in the experiment. These errors may result in an uncertain error of the sensor.

III. CHARACTERIZATION

Characterization experiments to identify and verify the basic characteristics of the incision sensor were performed using prototypes of the sensor. The intent of this experimentwas to validate the assumption that the electric potential on the conductive tape varies linearly according to the distance from the electrode. The linear relationship between the electric potential and distance is the fundamental principle employed by the incision sensor; thus, it should be rigorously validated experimentally. Moreover, the experimentally measured sensor output would be compared with the theoretical value, based on the equivalent circuit of the sensor. Fig. 8 shows the experimental setups for the characterization tests. The setup consists of 1D and 2D incision sensor prototypes, piercing guides, electric circuits, a metal needle, a power supply (DP30-05A, Toyotech Co., Incheon, South Korea), and a DAQ board (Arduino Uno, Arduino AG, Turin, Italy). In the experiment, the sensor prototypes were pierced with a metal needle at predefined reference points while measuring the output voltage of the sensor. The sensors were placed on top of a soft rubber layer to allow the needle to fully pierce the sensor. The measured outputs were labeled with the corresponding reference points, and finally, the relation between the output and the position on the sensor was derived using the experimental data. Piercing guides, fabricated with a 3D printer, were used to precisely guide the needle to predefined piercing points. The output of the voltage source was set to 5 V and was connected to the voltage input of the sensors. The voltage source and ground were directly connected to the electrode in 1D experiments and connected through the transistor in 2D experiments.

A. CHARACTERIZATION PROCEDURE

Three piercing experiments were conducted on 1D and 2D incision sensor prototypes. Figs. 9(a) and (b) show the dimension of the sensor prototypes and configuration of the reference piercing points for three different experimental cases. In the first experiment, the relationship between the sensor

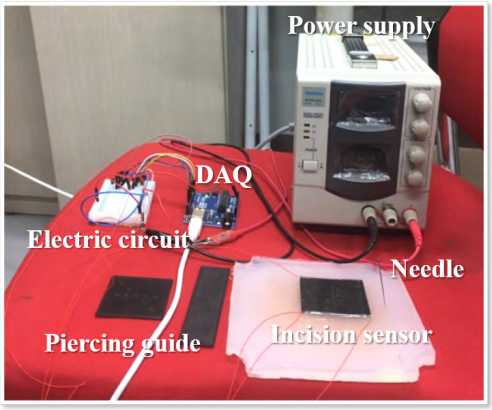

FIGURE 8. Experimental setup for the sensor characterization. The setup consists of an incision sensor, piercing guide, needle, electric circuit, and power supply. This setup is also used for the performance validation experiments.

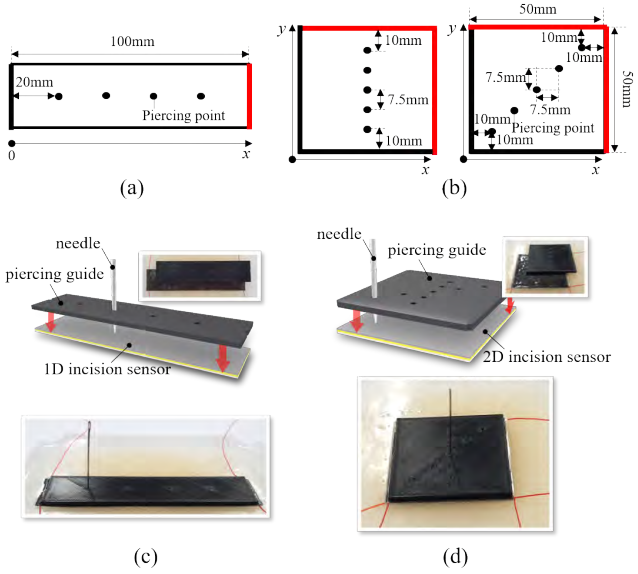

FIGURE 9. Characterization experiments. (a) Dimension of the incision sensor and reference pricking points used in the 1D characterization experiment. (b) Dimension of the incision sensor and reference pricking points used in the 2D characterization experiment. (c) Procedure of 1D characterization experiment. (b) Procedure of 2D characterization experiment.

output and the distance from the electrode for the 1D incision sensor was identified. A voltage source and ground were connected to the right and left electrodes of the sensor, respectively.

As shown in Fig. 9(a), the 1D coordinate frame was attached to the left end of the sensor. The coordinate values of the piercing points were calculated with respect to this frame using the measured sensor output voltage. The length and width of the sensor were 100 mm and 25 mm, respectively. Four points with the same interval (20 mm) were set as reference piercing points. These reference points were pierced with the metal needle. The output voltage of the sensor was measured and converted to the coordinate value using (12):

$$x_i = \frac{V_{q,i}}{V_r - V_g} L \tag{11}$$

where x_i is the estimated position of the i-th piercing point, $V_{q,i}$ is the measured sensor output at the i-th piercing point, and L is the length of the sensor (100 mm).

The second and third experiments were performed on the 2D incision sensor. Square-shaped sensor prototypes with side length 50 mm were used with two sets of reference piercing points, as shown in Fig. 9(b). The voltage source and ground were connected to the top-right and bottom-left electrodes, respectively, through the transistors. In the second experiment, five reference piercing-points were set in the vertical direction of the sensor with the same interval (7.5 *mm*). In the third experiment, five reference piercing-points were placed in the diagonal direction of the sensor with the interval $7.5\sqrt{2}$ *mm*. The outputs of the sensor were measured to validate the same assumption as in the 1D sensor characterization test. The electric potentials at the left, right, bottom, and top ends of the sensor were measured and used to calculate the coordinate values of the piercing points as follows:

$$x_i = \frac{V^x_{q,i}}{V^x_r - V^x_g} L^x, \quad y_i = \frac{V^y_{q,i}}{V^y_r - V^y_g} L^y \tag{12}$$

where (x_i, y_i) are the estimated coordinate values of the i-th piercing point, $(V^x_{q,i}, V^y_{q,i})$ are the measured sensor outputs at the i-th piercing point, and (L^x, L^y) are the lengths of the sensor in the x and y directions, respectively. V^x_g, V^x_r, V^y_g, and V^y_r are the electric potentials at the left, right, bottom, and top ends of the sensor. The mean value of the electric potentials measured at the bottom-left and top-left corners of the sensor was used for V^x_g, and the others were measured similarly for each sensor prototype. Seven sensor prototypes were used for each experimental case (total 21 prototypes). The sensor output on the three prototypes under identical experimental conditions were measured to validate the repeatability of the sensor characteristics and compared these with the theoretical value computed based on the equivalent circuit model.

B. CHARACTERIZATION RESULTS

Table 1 shows the output voltage of the sensor measured in the 1D characterization experiment compared with the theoretically computed value. The measured reference voltages V_g and V_r were 1.23 and 3.48 V on average, respectively, and the sensor output was found to linearly increase with position on the sensor. These experimental results confirm the fundamental assumption of the incision sensor that the electric potential on the driving layer increases linearly according to the displacement. There exists significant difference between measured sensor outputs and the theoretical value. The error was mainly caused by inaccurate estimation of V_g and V_r, thus these values should be adjusted for each sensor through calibration. Fig. 10 shows the estimated position of the piercing points. To convert the sensor output to the position, the experimentally measured reference voltages (V_g and V_r)

TABLE 1. Comparison of theoretical and experimental value of the sensor output in 1D characterization experiment.

x (mm)	Theoretical (V)	Experimental (V)	
		Average	SD
0	0.38 (V_g)	1.23 (V_g)	0.07
20	1.23	1.63	0.06
40	2.08	2.08	0.06
60	2.92	2.51	0.07
80	3.77	2.97	0.04
100	4.62 (V_r)	3.48 (V_r)	0.05

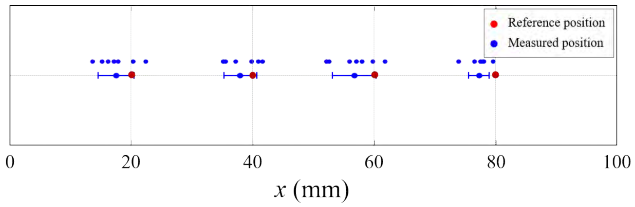

FIGURE 10. Characterization experimental results for the 1D incision sensor.

TABLE 2. Comparison of theoretical and experimental value of the sensor output in 2D characterization experiment of vertical incision.

Position (mm)		Theoretical (V)		Experimental (V) Average		SD	
x	y	x	y	x	y	x	y
0	0	0.69	0.69	0.87	1.03	0.03	0.05
25	10	2.11	1.26	2.01	1.49	0.06	0.04
25	17.5	2.11	1.68	2.03	1.83	0.03	0.07
25	25	2.11	2.11	2.02	2.19	0.04	0.07
25	32.5	2.11	2.53	2.01	2.57	0.02	0.04
25	40	2.11	2.95	2.05	2.83	0.07	0.05
50	50	3.52	3.52	3.12	3.32	0.03	0.03

were used. The estimated positions were slightly shifted to the left of the reference positions. The error of the position measurement was in the range from −7.88 to 2.39 mm. The standard deviations (SDs) of the position measurements ranged from 1.75–3.54 mm.

Table 2 shows the output voltage of the sensor measured in the 2D characterization experiment (vertical direction). The measured reference voltages V_g^x, V_g^y, V_r^x, and V_r^y were 0.87, 1.03, 3.12, and 3.32 V respectively. The x-directional output voltages were 2.03 ± 0.02 V, and the y-directional output voltage linearly increased in the range $1.49 - 2.83$ V. The differences between the theoretical and experimental values were smaller than the 1D experiments, but not negligible. Thus, it also requires calibration for each sensor.

Fig. 11 shows the measured piercing points (blue dots) with the reference points (red dots). The top-left figure shows the average of the measured points, while the others show the measured points from each sensor prototype. The average of the measured values was slightly shifted to the positive y-direction at all piercing points, and there seems to be a regular bias in the sensor position. However, the shift does not regularly arise in the data presented by each sensor prototype

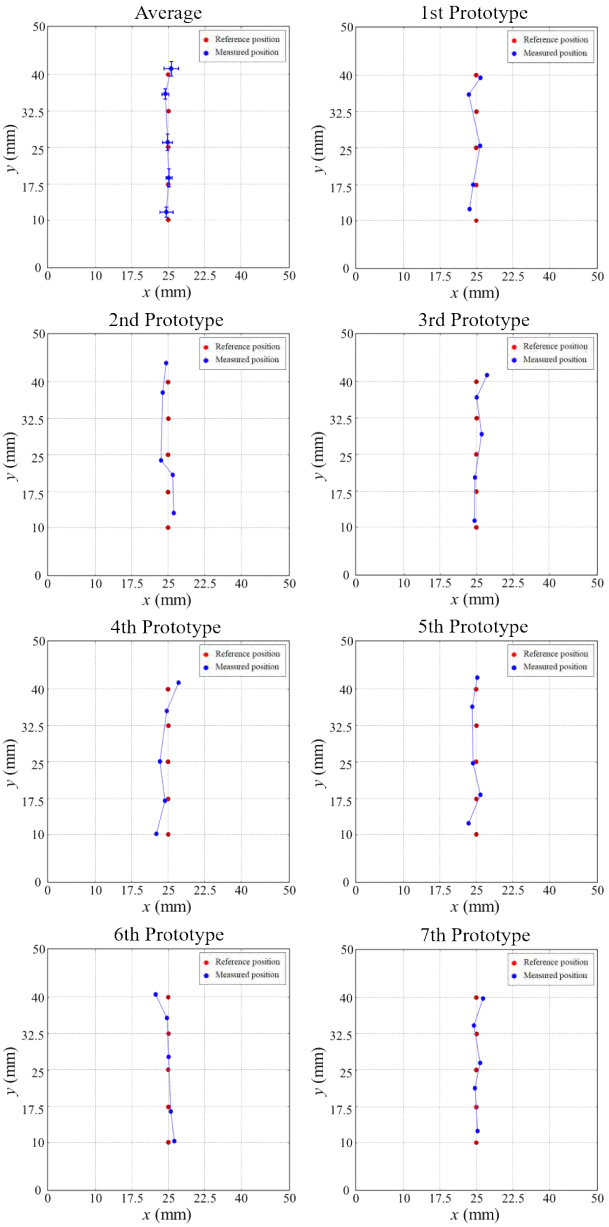

FIGURE 11. Characterization experimental results for the 2D incision sensor with piercing points in the vertical direction.

TABLE 3. Comparison of theoretical and experimental value of the sensor output in 2D characterization experiment of cross incision.

Position (mm)		Theoretical (V)		Experimental (V) Average		SD	
x	y	X	y	x	y	x	y
0	0	0.69	0.69	0.87	1.03	0.03	0.04
10	10	1.26	1.26	1.30	1.46	0.06	0.08
17.5	17.5	1.68	1.68	1.60	1.89	0.06	0.05
25	25	2.11	2.11	1.95	2.22	0.05	0.06
32.5	32.5	2.53	2.53	2.30	2.66	0.02	0.06
40	40	2.95	2.95	2.58	2.92	0.06	0.03
50	50	3.52	3.52	3.12	3.35	0.03	0.03

(rest of the figure) but rather seems more random. Thus, we cannot treat this error as a regular bias of the sensor, and the shift can be regarded as an uncertain measurement

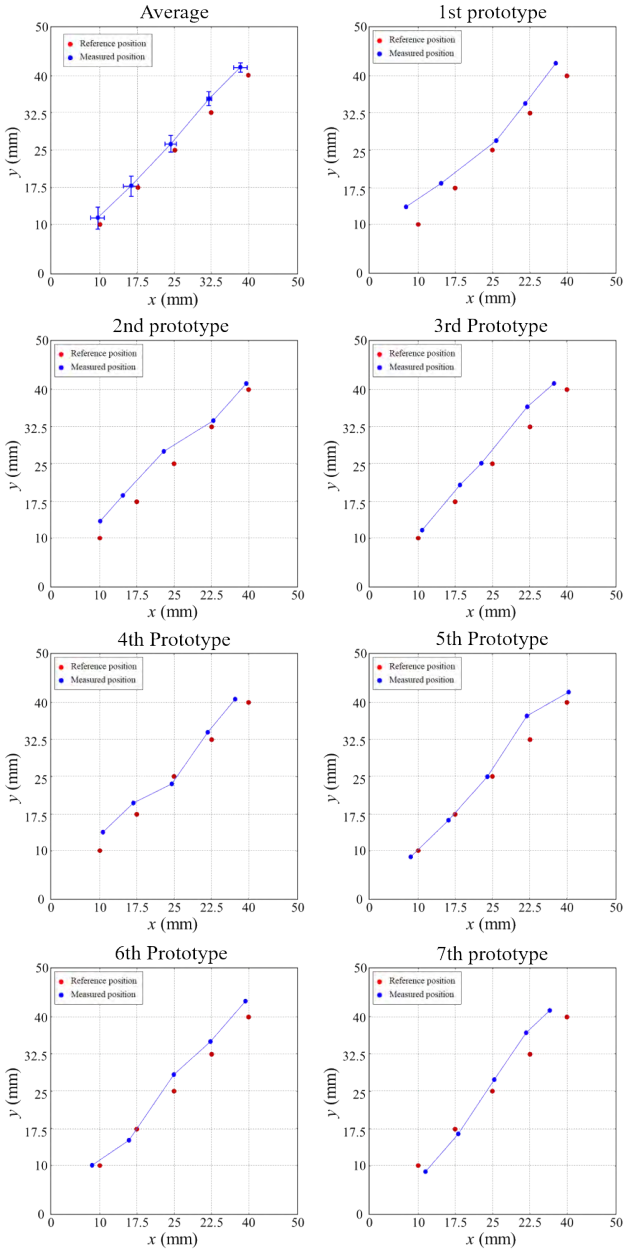

FIGURE 12. Characterization experimental results for the 2D incision sensor with piercing points in the vertical direction.

error for the proposed sensor. The amount of the error in the x-direction ranged from -0.69 mm and 0.49 mm, and the error in the y-direction ranged from 1.09 mm to 3.55 mm. The maximum error in Euclidean distance was 3.62 mm at the fourth piercing point ($x = 25$, $y = 32.5$).

Table 3 shows the output voltage of the sensor measured in the 2D characterization experiment (diagonal direction). The results were similar to those of the vertical direction experiment. The sensor outputs in the x- (1.30–2.58 V) and y- (1.46–2.92 V) directions linearly increase with piercing position.

Fig. 12 shows the measured piercing points with the reference points. Similar to the results for the vertical piercing, the average of the measured points were slightly shifted to the positive y-direction at all piercing points, but the shift does not regularly arise in the data of each sensor. The amount of error in the x-direction ranged from 0.35 mm to 1.70 mm, and the error in y-direction ranged from 0.39 mm to 2.88 mm. The maximum error in Euclidean distance was 2.92 mm at the fourth piercing point ($x = 32.5$, $y = 32.5$).

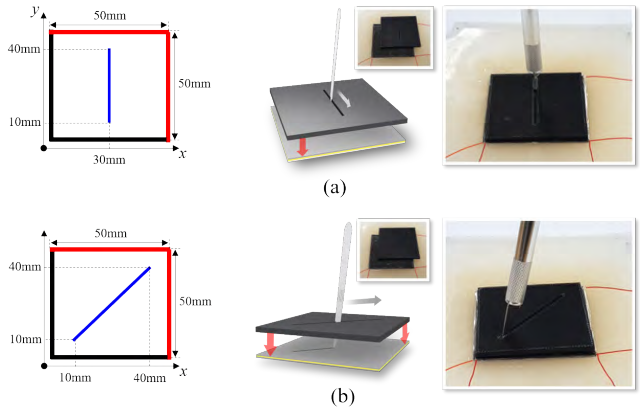

FIGURE 13. Incision experiments for preformation validation. (a) Dimension of reference incision trajectory in the vertical direction and experimental procedure. (b) Dimension of reference incision trajectory in the diagonal direction and experimental procedure.

IV. INCISION EXPERIMENTS

A. EXPERIMENTAL SETUP

The fundamental principle of the sensor (linear relationship between sensor output and position) was verified in the characterization experiments. In this section, the performance of the incision sensor was validated. The experimental setup was similar to the setup for the characterization shown in Fig. 8. In all, 7 incision sensor prototypes were prepared for vertical and cross-directional incision experiments each (14 prototypes in total). The incision guides corresponding to each experiment case were fabricated to guide the incision tool (metal knife) along the predefined reference path in the experiment. Fig. 13 shows the experimental conditions of the three incision experiments. In the first experiment, a 2D square incision sensor (side length = 50 mm) was incised vertically from the bottom ($x = 25$ mm, $y = 10$ mm) to the top ($x = 25$ mm, $y = 40$ mm), as shown in Fig. 13(a). In the second experiment, a 2D incision sensor with the same dimensions was incised in a diagonal direction from the bottom-left ($x = 10$ mm, $y = 10$ mm) to the top-right ($x = 40$ mm, $y = 40$ mm), as shown in Fig. 13(b).

B. EXPERIMENTAL RESULTS

Fig. 14 shows the results of vertical incision experiment. In the graph, the red dotted line represents the reference incision path, and the blue line represents the measured incision path. The narrow blue line is the measured incision path for each trial, and the bold solid blue line is the average value of the measured incision path. The measured incision path in each trial lies near the reference path in all 7 incision experiments, but it does not exactly match the refence path. The maximum error measured over all incision trials was

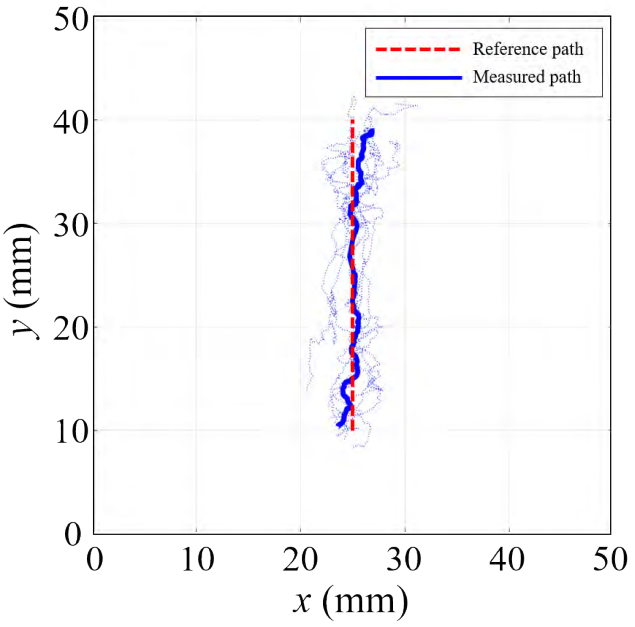

FIGURE 14. Results of the 2D incision experiment in the vertical direction.

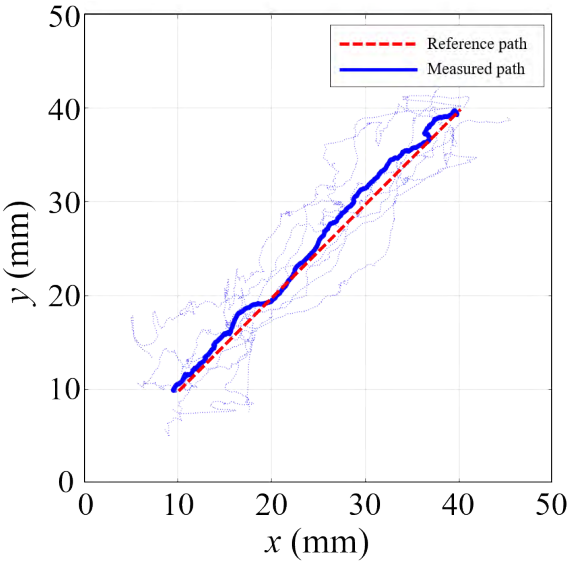

FIGURE 15. Results of the 2D incision experiment in the diagonal direction.

6.12 mm. However, the averaged incision path, presented in the bold blue line, converges to the reference path. The maximum error in the averaged incision path was 2.31 mm, and the root-mean-square error was 0.98 mm.

Fig. 15 shows the results of the cross-incision experiment. The results were similar to the vertical-incision experiment. The maximum error measured over all incision trials was 7.21 mm. The averaged incision path converges to the reference path, and the maximum error in the averaged incision path was 1.72 mm. The RMS error was 1.03 mm.

V. DISCUSSION AND CONCLUSION

In this study, incision sensors that can measure incision information in a plane, using the characteristics of conductive materials (Pouillet's law) were designed and developed. 1D and 2D incision sensors were fabricated and characterized using piercing experiments. Incision experiments were also performed to validate the performance of the sensor for incision measurement.

Based on the results obtained through the characterization experiments, this study confirmed that the sensor outputs and piercing positions have a quasi-linear relationship for 1D (horizontal direction) and 2D (vertical and diagonal directions) sensors. The results show that measuring positions in the x-coordinate, calculated from the output voltage of the 1D incision sensors is almost the same as that based on piercing positions. For the 2D sensor, the measured positions for vertical and diagonal piercing also show similar results. The measured positions in the piercing experiments were consistently slightly shifted toward the upper left, compared with the ideal, due to limitations in sensor fabrication. Errors in the fabrication procedure, such as misalignment between layers and inaccurate layer dimensions are evident. Furthermore, the conductive tape, which is fabricated with randomly dispersed conductive fibers, has locally inhomogeneous characteristics due to limitations in the fabrication process and conductive fiber characteristics. The contact resistance at the junction between electrodes and the conductive tape also varies among the prototypes, and results in an uncertain error of the sensor.

The results of the incision experiments are similar to those of the characterization experiments. In the first experiment on the 2D sensor, the sensor outputs for the y-coordinate linearly increased along the incision, while for the x-coordinate (transverse to the incision), they were nearly constant. In the second experiment (diagonal incision), sensor outputs for both x- and y-coordinates increased. The measured incision paths in terms of the x- and y-coordinates for the vertical and diagonal directions were similar to the reference path. The results were slightly shifted, with RMS errors of 0.98 mm and 1.03 mm for the vertical and diagonal measurements, respectively. The mechanical resistance due to the embedded sensor into the artificial skin was also measured. The results show that the reaction force with the sensor is larger by about 19% than without the sensor.

The main contribution of this work is to establish the incision sensor principle (driving layer and sensing layer with conductive materials, dielectric layer, conductive tool to incise) and validate the sensor principle with characterization and incision experiments for 1D and 2D sensors. The results demonstrate the feasibility of the proposed sensor and its applicability to cricothyrotomy training simulation in measuring the incision path made by the trainee. Current research in this area involves improving the linearity and repeatability of the incision sensor. In particular, we are exploring alternate designs that stabilize the transistor behavior across variations in temperature and between individuals, as well as, between unmatched transistors. In addition, the Arduino, a data acquisition device, allows us to measure multiple analog voltages, so the sensor could be modified to

directly measure, not only the sensing layer electrode voltage, but also the driving layer electrode voltages, eliminating the need to estimate V_{tr}.

We are also developing an augmented-reality cricothyrotomy training simulator using the proposed sensors, integrating them with the neck skin and cricothyroid membranes of the physical dummy. Furthermore, we believe that the sensor can be used to measure suturing position (metal needle piercing), based on the results of the characterization experiments. Thus, this sensor can be applied to develop a suturing training simulator with similar technologies.

REFERENCES

[1] D. S. J. Elliott, P. A. Baker, M. R. Scott, C. W. Birch, and J. M. D. Thompson, "Accuracy of surface landmark identification for cannula cricothyroidotomy," *Anaesthesia*, vol. 65, no. 9, pp. 889–894, Sep. 2010. doi: 10.1111/j.1365-2044.2010.06425.x.

[2] M. G. Katos and D. Goldenberg, "Emergency cricothyrotomy," *Operative Techn. Otolaryngol.-Head Neck Surg.*, vol. 18, no. 2, pp. 110–114, Jun. 2007, doi: 10.1016/j.otot.2007.05.002.

[3] C. Frerk and C. Frampton, "Cricothyroidotomy; Time for change," *Anaesthesia*, vol. 61, no. 10, pp. 921–923, Oct. 2006. [Online]. Available: http://onlinelibrary.wiley.com/doi/10.1111/j.1365-2044.2006.04798.x/epdf

[4] D. T. Wong, A. J. Prabhu, M. Coloma, N. Imasogie, and F. F. Chung, "What is the minimum training required for successful cricothyroidotomy?: A study in mannequins " *Anesthesiology*, vol. 98, no. 2, pp. 349–353, Feb. 2003. [Online]. Available: http://anesthesiology.pubs.asahq.org/article.aspx?articleid= 1942795

[5] J. B. Fortune, D. G. Judkins, D. Scanzaroli, K. B. McLeod, and S. B. Johnson, "Efficacy of prehospital surgical cricothyrotomy in trauma patients," *J. Trauma*, vol. 42, no. 5, pp. 832–838, 1997. [Online]. Available: https://insights.ovid.com/pubmed?pmid=9191664

[6] J. Cho *et al.*, "Comparison of manikin versus porcine models in cricothyrotomy procedure training," *Emergency Med. J.*, vol. 25, no. 11, pp. 732–734, Nov. 2008. [Online]. Available: http://emj.bmj.com/content/25 /11/732.long#

[7] C. Keller and J. Brimacombe, "The intubating laryngeal mask airway in fresh cadaversvs paralysed anesthetised patients," *Can. J. Anesthesia*, vol. 46, no. 11, pp. 1067–1069, Nov. 1999. [Online]. Available: https://link.springer.com /content/pdf/10.1007

[8] A. Mirzazadeh, N. Ostadrahimi, S. M. Ghalandarpoorattar, and F. Asghari, "Teaching endotracheal intubation on the recently deceased: Opinion of patients and families," *J. Med. Ethics Hist. Med.*, vol. 7, no. 5, pp. 2–6, Mar. 2014. [Online]. Available: https://www.ncbi.nlm.nih.gov/pmc/articles/PMC4263388/pdf/jmehm-7-5.pdf

[9] S. S. Varaday, S. M. Yentis, and S. Clarke, "A homemade model for training in cricothyrotomy," *Anaesthesia*, vol. 59, no. 10, pp. 1012–1015, Oct. 2004, doi: 10.1111/j.1365-2044.2004.03810.x.

[10] C. B. Custalow, J. A. Kline, J. A. Marx, and M. R. Baylor, "Emergency department resuscitative procedures: Animal laboratory training improves procedural competency and speed," *Acad. Emergency Med.* vol. 9, no. 6, pp. 575–586, Jun. 2002. doi:10.1197/aemj.9.6.575.

[11] F. A. C. S. Netto, P. Zacharias, R. F. F. Cipriani, M. De M. Constantino, M. Cardoso, and R. A. Pereira, "A porcine model for teaching surgical cricothyridootomy," *Revista do Colégio Brasileiro de Cirurgiões*, vol. 42, no. 3, pp. 193–196, Jun. 2015. [Online]. Available: http://www.scielo.br/pdf/rcbc/v42n3/0100-6991-rcbc-42-03-00193.pdf

[12] A. J. Byrne, P. J. Hilton, and J. N. Lunn, "Basic simulations for anaesthetists A pilot study of the ACCESS system," *Anaesthesia*, vol. 49, no. 5, pp. 376–381, May 1994, doi: 10.1111/j.1365-2044.1994.tb03466.x.

[13] M. W. P. Goodwin and G. W. G. French, "Simulation as a training and assessment tool in the management of failed intubation in obstetrics," *Int. J. Obstetric Anesthesia*, vol. 10, no. 4, pp. 273–277, Oct. 2001. [Online]. Available: https://www.science direct.com/science/article/pii/S0959289X01908581?via

[14] K. R. Stringer, S. Bajenov, and S. M. Yentis, "Training in airway management," *Anaesthesia*, vol. 57, no. 10, pp. 967–983, Oct. 2002, doi: 10.1046/j.1365-2044.2002.02830.x.

[15] V. Chopra, B. J. Gesink, J. J. De, J. G. Bovill, J. Spierdijk, and R. Brand, "Does training on an anaesthesia simulator lead to improvement in performance," *Br J Anaesth.*, vol. 73, no. 3, pp. 293–297, Sep. 1994. [Online]. Available: https://www.ncbi.nlm.nih.gov/pubmed/7946851

[16] D. M. Gaba and A. DeAnda, "A comprehensive anesthesia simulation environment. Re-creating the operating room for research and training," *Anesthesiology*, vol. 69, no. 3, pp. 387–394, Sep. 1988.

[17] L. W. Siu *et al.*, "High-fidelity simulation demonstrates the influence of anesthesiologists' age and years from residency on emergency cricothyroidotomy skills," *Anesthesia Analgesia*, vol. 111, no. 4, pp. 955–960, Oct. 2010. [Online]. Available: https://insights.ovid.com/pubmed?pmid=20736429

[18] D. Silvera-Tawil, D. Rye, and M. Velonaki, "Artificial skin and tactile sensing for socially interactive robots: A review," *Robot. Auton. Syst.*, vol. 63, no. 3, pp. 230–243, Jan. 2015. [Online]. Available: https://www.sciencedirect.com/science/article/pii/S0 921889014001833#

[19] A. Spanu *et al.*, "A high-sensitivity tactile sensor based on piezoelectric polymer PVDF coupled to an ultra-low voltage organic transistor," *Organic Electron.*, vol. 36, pp. 57–60, Sep. 2016. [Online]. Available: https://www.sciencedirect.com/science/article/pii/S1566119916302300#

[20] F. L. Hammond, III, R. K. Kramer, Q. Wan, R. D. Howe, and R. J. Wood, "Soft tactile sensor arrays for force feedback in micromanipulation," *IEEE Sensors J.*, vol. 14, no. 5, pp. 1443–1452, May 2014. [Online]. Available: http://ieeexplore.ieee.org/stamp/stamp.jsp?tp=&arnumber=6701139

[21] B. Sümer and I. M. Koc, "Fabrication of a flexible tactile sensor with micro-pillar array," *Procedia Eng.*, vol. 120, pp. 134–137, 2015. [Online]. Available: https://www.sciencedirect.com/science/article/pii/S187770581502247X

[22] K. F. Lei, K.-F. Lee, and M.-Y. Lee, "A flexible PDMS capacitive tactile sensor with adjustable measurement range for plantar pressure measurement," *Microsyst. Technol.*, vol. 20, no. 7, pp. 1351–1358, 2014. [Online]. Available: https://link.springer.com/article/10.1007/s00542-013-1918-5

[23] E. V. Eason, E. W. Hawkes, M. Windheim, D. L. Christensen, T. Libby, and M. R. Cutkosky, "Stress distribution and contact area measurements of a gecko toe using a high-resolution tactile sensor," *Bioinspiration Biomimetics*, vol. 10, no. 1, p. 016013, Feb. 2015. [Online]. Available: http://iopscience.iop.org/article/10.1088/1748-3190/10/1/016013/pdf

[24] A. Drimus, G. Kootstra, A. Bilberg, and D. Kragic, "Design of a flexible tactile sensor for classification of rigid and deformable objects," *Robot. Auton. Syst.*, vol. 62, no. 1, pp. 3–15, Jan. 2014. [Online]. Available: https://www.sciencedirect.com/science/article/pii/S092188901200125X

[25] R. P. Bruce and M. G. William, "Emergency surgical cricothyroidotomy: 24 successful cases leading to a simple 'scalpel–finger–tube' method," *Emergency Med. Austral.*, vol. 24, no. 1, pp. 23–30, Feb. 2012. [Online]. Available: https://emcrit.org/wp-content/uploads/2014/08

[26] D. S. J. Elliott, P. A. Baker, M. R. Scott, C. W. Birch, and J. M. D. Thompson, "Accuracy of surface landmark identification for cannula cricothyroidotomy, *Anaesthesia*, vol. 65, no. 9, pp. 889–894, Sep. 2010, doi:10.1111/j.1365-2044.2010.06425.x.

[27] H. H. Berger, "Contact resistance and contact resistivity," *J. Electrochem. Soc.* vol. 119, no. 4, pp. 507–514, 1972.

[28] A. Venugopal, L. Colombo, and E. M. Vogel, "Contact resistance in few and multilayer graphene devices," *Appl. Phys. Lett.*, vol. 96, no. 1, p. 013512, 2010, doi: 10.1063/1.3290248.

BUMMO AHN received the master's and Ph.D. degrees from the Department of Mechanical Engineering, Korea Advanced Institute of Science and Technology, Daejeon, South Korea, in 2011.

He is currently the Principal Researcher of the Robotics Research and Development Group, Korea Institute of Industrial Technology, Ansan, South Korea. He is also appointed as an Associate Professor with the Robotics and Virtual Engineering, University of Science and Technology, Daejeon, South Korea. His current research interests include medical robotics, biomechanics, and rehabilitation.

WOONJAE CHOI received the B.S. degree in mechanical engineering from Incheon National University, Incheon, South Korea, in 2018.

He is currently pursuing the M.S. degree in robotics and virtual engineering with the University of Science and Technology, Daejoen, South Korea. He is also a Research Student with the Korea Institute of Industrial Technology, Ansan, South Korea.

MARK P. OTTENSMEYER received the master's and Ph.D. degrees in mechanical engineering from the Massachusetts Institute of Technology, Cambridge, MA, USA, in 2001.

He is currently the Director of the Medical Device and Simulation Laboratory (formerly Simulation Group), Massachusetts General Hospital. He is also appointed as an Assistant Professor with the Harvard Medical School. His current research interests include medical simulation, medical robotics, and application of 3D printing to surgical planning.

HOERYONG JUNG received the B.S. degree from the Department of Mechanical Engineering, Konkuk University, Seoul, South Korea, in 2006, and the master's and Ph.D. degrees from the Department of Mechanical Engineering, Korea Advanced Institute of Science and Technology, Daejeon, South Korea, in 2007 and 2012, respectively. He has worked for the Central Research Institute, Samsung Heavy Industries, Daejeon, from 2013 to 2017. He is currently an Assistant Professor with the Department of Mechanical Engineering, Konkuk University. His current research interests include medical simulation, haptics, and physics-based real-time simulation.